Journal of Instrumentation

Automated identification of the lung contours in positron emission tomography

PUBLISHED BY IOP PUBLISHING FOR SISSA MEDIALAB

RECEIVED: *October 12, 2012*
ACCEPTED: *February 4, 2013*
PUBLISHED: *March 18, 2013*

TECHNICAL REPORT

14th INTERNATIONAL WORKSHOP ON RADIATION IMAGING DETECTORS,
1–5 JULY 2012,
FIGUEIRA DA FOZ, PORTUGAL

Automated identification of the lung contours in positron emission tomography

F. Nery,[a] J. Silvestre Silva,[b,c,1] N.C. Ferreira,[a,d] F.J. Caramelo[d] and R. Faustino[a,d]

[a] *ICNAS - Institute of Nuclear Sciences Applied to Health, University of Coimbra, Coimbra, Portugal*
[b] *Instrumentation Center, Faculty of Sciences and Technology, University of Coimbra, Coimbra, Portugal*
[c] *School of Technology and Management, Polytechnic Institute of Portalegre, Portalegre, Portugal*
[d] *IBILI - Institute of Biomedical Research in Light and Image, Faculty of Medicine, University of Coimbra, Coimbra Portugal*

E-mail: jsilva@ci.uc.pt

ABSTRACT: Positron Emission Tomography (PET) is a nuclear medicine imaging technique that permits to analyze, in three dimensions, the physiological processes *in vivo*. One of the areas where PET has demonstrated its advantages is in the staging of lung cancer, where it offers better sensitivity and specificity than other techniques such as CT.

On the other hand, accurate segmentation, an important procedure for Computer Aided Diagnostics (CAD) and automated image analysis, is a challenging task given the low spatial resolution and the high noise that are intrinsic characteristics of PET images.

This work presents an algorithm for the segmentation of lungs in PET images, to be used in CAD and group analysis in a large patient database. The lung boundaries are automatically extracted from a PET volume through the application of a marker-driven watershed segmentation procedure which is robust to the noise. In order to test the effectiveness of the proposed method, we compared the segmentation results in several slices using our approach with the results obtained from manual delineation. The manual delineation was performed by nuclear medicine physicians that used a software routine that we developed specifically for this task. To quantify the similarity between the contours obtained from the two methods, we used figures of merit based on region and also on contour definitions. Results show that the performance of the algorithm was similar to the

[1] Corresponding author.

doi:10.1088/1748-0221/8/03/C03018

performance of human physicians. Additionally, we found that the algorithm-physician agreement is similar (statistically significant) to the inter-physician agreement.

KEYWORDS: Gamma camera, SPECT, PET PET/CT, coronary CT angiography (CTA); Medical-image reconstruction methods and algorithms, computer-aided so

2013 JINST 8 C03018

Contents

2013 JINST 8 C03018

1 Introduction

The possibility of analyzing, quantitatively, the evolution of lung cancer with PET can be made much more powerful if CAD and other automatic tools are used, easing the physician's task of detecting and measuring features in a large number of tomographic images. Therefore, it is of paramount importance to develop algorithms requiring minimal or no human interaction to speed up the process of mining the information from the PET images.

The initial step required for this process is to define the limits of the organ of interest, i.e., to perform the segmentation. The possibility of automatically defining the lung region as a first step for measuring and classifying with greater detail this organ and its lesions is a useful tool in the understanding of the disease and its therapies.

Furthermore, if combined with CT-based lung segmentation, PET lung segmentation can be also useful in the interpretation of possible artefacts due to movement and/or attenuation, and in the assessment of these data corrections.

The automatic segmentation can help the physician to observe the contours of the lungs superimposed on the original slice, allowing a visual assessment of the lung contours in adjacent slices. It also allows the comparison of equivalent slices in exams acquired in different instances of time (such as exams acquired 3 months apart for therapy assessment). Our method permits to calculate the lung area and volume, and therefore allows, in case of tumors being present, to evaluate the evolution of peripheral lung tumors (if their area/volume has increased or decreased).

1.1 State of the art

Several approaches have been proposed by many authors for the segmentation of PET images, namely concerning the segmentation of tumors in oncology using the 18F-fluorodeoxyglucose (FDG) PET tracer.

Jentzen et al. [1] and Kanakatte et al. [2] applied, respectively, iterative and fixed-value threshold techniques which allow to compute the volume of the tumors. Tridimensional region growing methods have also been used by Ballangan et al. [3] for the definition of lung tumor boundaries. Other approaches include the use of deformable models for the segmentation of the liver [4], in human patients and for the myocardium [5] in small animals. Semi-automatic [6] and automatic [7] graph-based approaches were also employed for segmentation of anatomical structures using functional information from PET scans. We improved the results of the watershed segmentation by providing markers which "guide" the growth of areas of interest during the segmentation procedure. Although the watershed segmentation has already been used in other imaging modalities, our goal was to segment the lungs in PET imaging which is a more challenging task compared to other modalities due to the low signal to noise ratio. The use of segmentation markers turned out to be essential in order to deal with this strong noise component.

Most recent segmentation methods based in deformable models, as parametric models or geometric models are used to identify not only the lungs [8–14] but also heart regions [15–17] vascular or neural structures [18] and to assist the classification of pathologies [19, 20].

2 Methods

The concept of watershed segmentation is based on the visualization of a gray-level image as a topographic surface. The 3D space is composed by the two spatial coordinates in addition to the intensity of the image, which determines the height of the landscape. The algorithm mimics the behavior of a flood where the water, starting from the surface base from below (regional minima) gradually climbs the peaks. When the water rising from two distinct catchment basins is about to merge, a virtual dam is built to prevent the merging. The algorithm stops when only the top of the dams are "visible" and thus, the "lines" formed by them correspond to the connected boundaries extracted by the algorithm. To avoid oversegmentation, a common issue in the watershed segmentation, markers should be used. The markers are connected components which help to identify both the foreground and the background structures.

2.1 Segmentation algorithm

Our approach is based in the concept of *Marker-driven Watershed Segmentation* [21] for the computation of the boundaries of the lungs in PET. This section discusses the details of our method.

2.1.1 Overview

The same acquisition protocol was used for all patients, with an injected dose proportional to the bodyweight of the patient (5 MBq/kg). An elapsed time of 40 minutes between the dose administration and the scanning allows for an adequate biodistribution. The average scan time is 25-30 minutes (2 min/frame).

2013 JINST 8 C03018

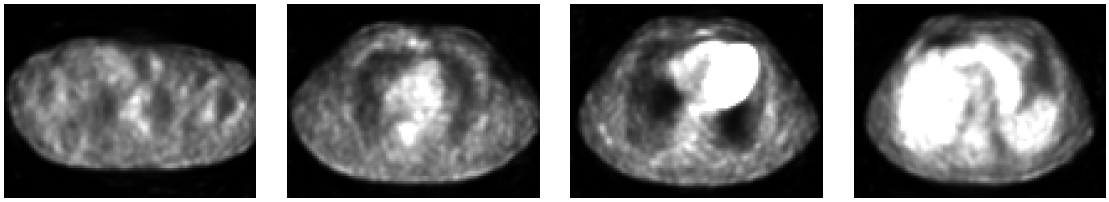

Figure 1. Examples of PET slices of the pulmonary region, going from the apex of the lung (left) to its base (right).

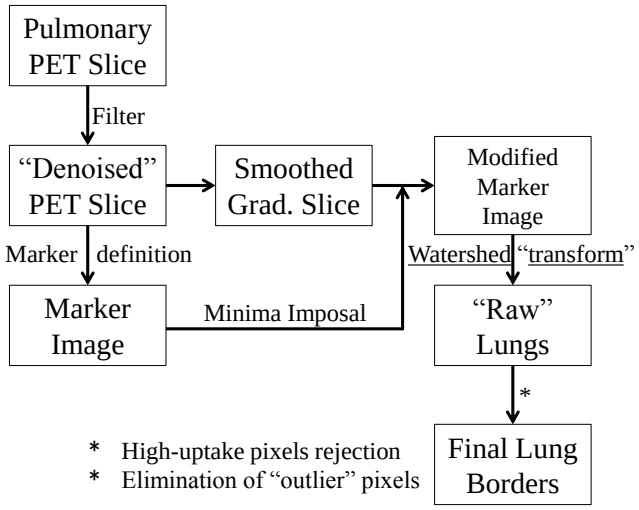

Figure 2. Overview of the segmentation algorithm.

Several examples of FDG-PET transaxial slices (144×144 pixels) of the pulmonary region, from the apex to the base of the lung, are given in figure 1. For a better visualization of the low uptake structures (such as the lungs), all PET images in this section are cropped and shown with a Standardized Uptake Value (SUV), which is the most commonly used measure to differentiate malignant from benign tumors and assess the efficacy of therapy [22], display ranging from a SUV of 0 to 1.

The first step of our algorithm is a filtering operation (see figure 2). We used a Wiener adaptive filter using a neighborhood of size 5×5 (empirically determined) to suppress high frequency noise. All the necessary markers are computed using the filtered slice (*"Denoised" PET slice* in figure 2), which are then imposed as the only regional minima into the smoothed gradient of the filtered slice (*Smoothed Grad. Slice* in figure 2), which is a new image, derived from the filtered one, where the borders are enhanced. We then compute the watershed lines of the *Modified Marker Image* (figure 2). Several post-processing steps are then applied in order to improve the segmentation results, yielding the *Final Lung Borders* (figure 2).

2.1.2 Determination of the markers

We defined two types of markers: *internal* markers (figure 3 b)), associated with the regions of interest, and *external* markers (figure 3 c)), associated with the background.

2013 JINST 8 C03018

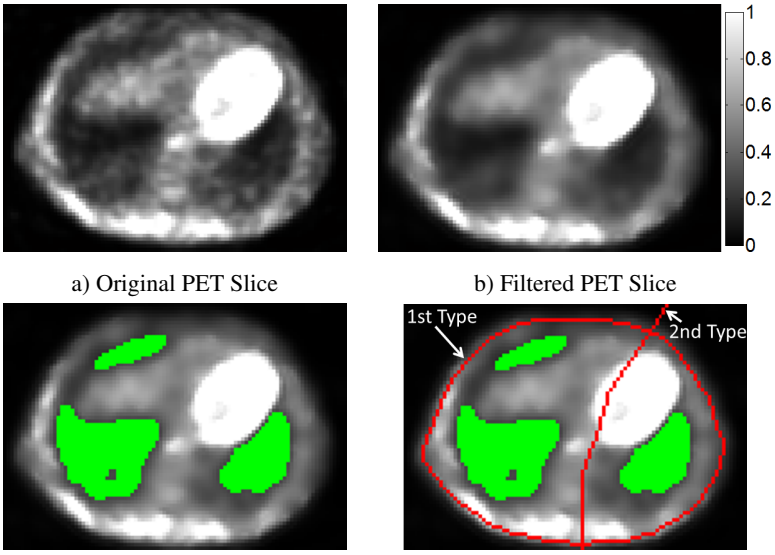

a) Original PET Slice b) Filtered PET Slice

c) Internal Markers d) Internal and External Markers

Figure 3. Example PET slice for the determination of the markers.

Initially, the internal markers are defined taking into account the low intensity (low uptake) of the lungs, using a threshold operation with the cut value T_{lu}. Then, the distance, d (number of pixels), between the border of the patients' body and the largest low uptake structures is computed and the border is dilated d times in order to reject non-lung regions which are also characterized by a low uptake and are close to the skin surface. The computation of the internal markers ends with a series of morphological operations, such as erosions and dilations, for a more accurate representation of the foreground structures.

The external markers prevent an excessive growth during the watershed transformation stage. The first type is derived from the boundary of the body which is computed during the definition of the internal markers by performing $\frac{1}{4}\times d$ dilations and using only the set of pixels corresponding to the inner border of the dilated object. The second type of external marker is computed as resulting watershed line from the distance transform of the internal markers.

2.1.3 Additional steps

Having computed all the necessary markers, the next step is their imposition into the smoothed gradient of the filtered slice. The watershed lines of the modified gradient image are then computed.

In order to improve the segmentation results, two additional steps were implemented. Sometimes, an excessive growth may include several high-intensity pixels near the border of the heart. These pixels are identified by applying a threshold procedure whose cut value is given by $2\times T_{lu}$ (see subsection 2.1.2). This step is illustrated in figure 4.

The last stage is the removal of *outlier* pixels. For a specific PET slice, the segmentation results of the two adjacent slices (in each direction) are considered. The binary areas enclosed by segmentation results in the adjacent slices are summed and the 1-valued pixels in the result of this operation (i.e. the pixels that only are present in 1 out of the 5 slices) are considered *outliers*, which

2013 JINST 8 C03018

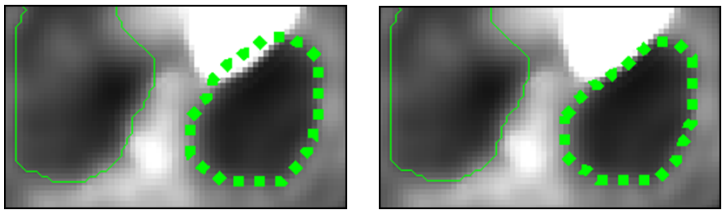

Figure 4. Improvement of the lung border near the heart. This image corresponds to a zoomed version of a slice where this improvement is mandatory with the result of the operation being clearly visible.

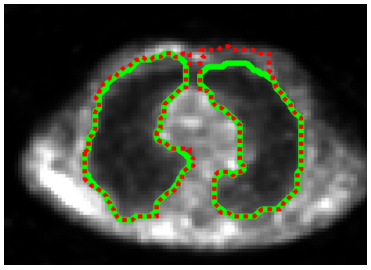

Figure 5. Lung borders: before (dashed) and after (solid) the removal of outlier pixels.

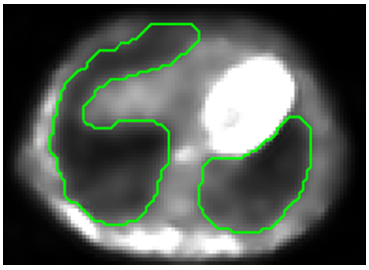

Figure 6. Final lung borders corresponding to the example slice.

are then removed. The lung areas are then smoothed using morphological operations. The results of this step are illustrated in figure 5.

The final lung borders (figure 2) corresponding to the slice represented in figure 3 a) are given in figure 6.

2.2 Performance assessment

An assessment of the performance of our method was conducted using 2 randomly selected patients (from a group of 10). From the selected patients, 30 randomly selected pulmonary slices (60 lung contours) were evaluated. The lung borders, which are the output of our algorithm were compared to the corresponding manual delineations performed by two nuclear medicine physicians. The lung contours were compared using one distance-based (Pratt figure of Merit, F_{Pratt} [23]) and one region-based (Dice Similarity Coefficient, DSC [24]) similarity metrics. The F_{Pratt} and the DSC are given, respectively by eq. (2.1) and eq. (2.2).

$$F_{Pratt} = \frac{1}{N}\sum_{i=1}^{N}\frac{1}{1+\alpha\times d_i^2} \qquad (2.1)$$

$$DSC = \frac{2|A\bigcap B|}{|A|+|B|} \qquad (2.2)$$

Both metrics vary between 0 and 1, where 1 indicates the complete overlapping of both contours. The term N and d_i are, respectively, the number of pairs of corresponding points and the distance between them. The normalization parameter α was set to $\frac{1}{9}$ so that F_{Pratt}=0.5 for d_i=3 pixels. The DSC helps to quantitatively evaluate the amount of intersection between the areas which are enclosed by the contours obtained in two images.

After verifying the violation of the assumptions for statistical parametric testing, we evaluated the comparisons between the algorithm and the two physicians by a Friedman test (α=0.05) fol-

2013 JINST 8 C03018

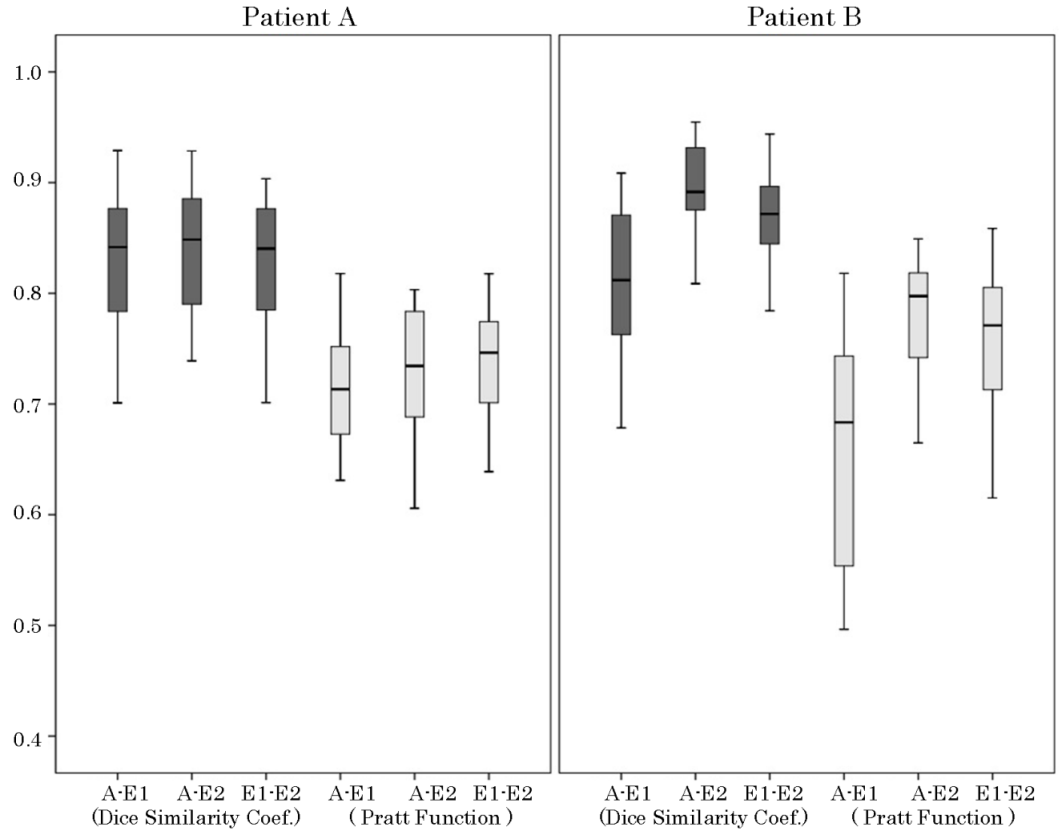

Figure 7. Boxplots of DSC and F_{Pratt} for the different segmentation procedures.

lowed by Wilcoxon paired sample tests. We also checked the association between segmentation procedures with the Spearman correlation coefficient.

3 Results and discussion

The results of comparisons using the two referred figures of merit in both patients are given in figure 7. The labelling convention is as follows:

- **A-E1** and **A-E2:** Algorithm-Physician comparison;
- **E1-E2:** Inter-physician comparison;

Results of the comparisons for the two lungs (patients) are different. In patient A there are no statistically significant differences ($\chi^{(2)}$=0.364; p=0.834 for DSC; $\chi^{(2)}$=1.727; p=0.422 for F_{Pratt}) between the comparison groups. However, in patient B there are statistically significant differences ($\chi^{(2)}$=32.813; p¡0.0001 for DSC; $\chi^{(2)}$=29.688; p¡0.0001 for F_{Pratt}).

In patient B, there are statistically significant differences (Z¡-2.5; p¡0.010) for DSC and F_{Pratt} between all the groups except for F_{Pratt} between E1-E2 vs. A-E2 (Z=-1.477; p=0.140).

The correlation coefficient (CC) between measures is statistically significant in patient B (DSC A-E1 vs. A-E2: CC=0.532; p=0.002; DSC A-E1 vs. E1-E2: CC=0.676; p¡0.0001; F_{Pratt} A-E1

2013 JINST 8 C03018

vs. A-E2: 0.503; p=0.003; F_{Pratt} A-E1 vs. E1-E2: 0.503; p¡0.0001), suggesting that either the physicians and the algorithm perform better in some slices and worse in others, which can explain the differences detected before. In patient A, there is no association between the variables (p¿0.05) which shows that segmentation procedures are independent.

The worst cases (greatest dissimilarity between the algorithm results and manual delineations) were verified to belong to apex slices. This was expected given the considerable influence of the respiratory movements in this particular region. The poor image resolution, large noise component, significant blurring and lack of anatomical information which characterize PET images also made the segmentation of anatomical structures a very challenging task, even for the manual delineations, as was confirmed by the large variability that was found between manual delineations. Nevertheless, the examination of the segmentation results suggests that when both physicians agree (to a certain extent) upon the location of the lung borders, the algorithm produces smaller errors in the segmentation.

4 Conclusions

We propose a fully automatic algorithm for the segmentation of the lungs using solely data from PET scans. The proposed method produces contours similar to the ones drawn by the physicians. The performance of our method is identical to the performance of two physicians (when compared with our method) and to the performance of the physicians among them. These results suggest that our method can be applied in the clinical environment for a final evaluation.

References

[1] W. Jentzen, L. Freudenberg, E. G. Eising, M. Heinze, W. Brandau and A. Bockisch, *Segmentation of PET volumes by iterative image thresholding*, *J. Nucl. Med.* **48** (2007) 108.

[2] A. Kanakatte, N. Mani, B. Srinivasan and J. Gubbi, *Pulmonary tumor volume detection from Positron Emission Tomography images*, in proceedings of *Int. Conf. Biomed. Eng. Inf. (BMEI)*, May, 27–30 (2008)

[3] C. Ballangan, X. Wang, S. Eberl, Y. Yin and D. Feng, *Automated delineation of lung tumors in PET images based on monotonicity and a tumor-customized criterion*, *IEEE Trans. Inf. Technol. Biomed.* **15** (2011) 691.

[4] C.-Y. Hsu, C.-Y. Liu and C.-M. Chen, *Automatic segmentation of liver PET images*, *Comput. Med. Imag. Grap.* **32** (2008) 601.

[5] R. Dedić, M. Allili and R. Lecomte, *Unsupervised cardiac PET image segmentation*, in proceedings of *18th International conference on systems, signals and image processing (IWSSIP)*, June, 16–18, 2011, Dept. de Math., Univ. de Sherbrooke, Sherbrooke, QC, Canada.

[6] U. Bağci, J. Yao, J. Caban, E. Turkbey, O. Aras and D. J. Mollura, *A graph-theoretic approach for segmentation of PET images*, in proceedings of *Annual International Conference of the IEEE Engineering in Medicine and Biology Society (EMBS)*, August, 30, 2008–September, 1, 2008, Boston, Massachusetts, USA.

[7] D. Onoma, S. Ruan, I. Gardin, G. Monnehan, R. Modzelewski and P. Vera, *3D random walk based segmentation for lung tumor delineation in PET imaging*, in proceedings of *9th IEEE International Symposium on Biomedical Imaging (ISBI)*, May, 2–5, 2012, Barcelona, Spain.

2013 JINST 8 C03018

[8] J.S. Silva, B.S. Santos, A. Silva and J. Madeira, *A Level-Set Based Volumetric CT Segmentation Technique: A Case Study with Pulmonary Air Bubbles*, in proceedings of *International Conference on Image Analysis and Recognition (ICIAR)*, September, 29, 2004–October, 1, 2004, Porto, Portugal.

[9] J.S. Silva, A. Silva, B.S. Santos and J. Madeira, *Detection and 3D representation of pulmonary air bubbles in HRCT volumes*, *Med. Imag.* **5031** (2003) 430.

[10] J. Cancela, J.S. Silva and L. Teixeira *Intra-Patient Registration Methods for Thoracic CT Exams*, in proceedings of *2nd International Conference on Bio-inspired System and Signal Processing (BIOSIGNALS 2009)*, January, 14–17, 2009, Porto, Portugal.

[11] J.S. Silva, A. Silva and B.S. Santos, *Image Denoising Methods for Tumor Discrimination in High-Resolution Computed Tomography*, *J. Digit. Imag.* **24** (2011) 464.

[12] J.S. Silva, J. Cancela and L. Teixeira, *Fast volumetric registration method for tumor follow-up in pulmonary CT exams*, *J. Appl. Clin. Med. Phys.* **12** (2011) 362.

[13] J. Cancela, J.S. Silva and L. Teixeira *Fast Intra-Patient 3D Registration Method for Pulmonary CT Exams*, in proceedings of *3rd Iberian Conference in Systems and Information Technologies (CISTI)*, 2008, Vigo, Spain.

[14] J.S. Silva, A. Silva and B.S. Santos, *A volumetric pulmonary CT segmentation method with applications in emphysema assessment*, *Med. Imag.* **6143** (2006) 885.

[15] S.G. Antunes, J.S. Silva and J. B. Santos, *A new level set based segmentation method for the four cardiac chambers*, in proceedings of *5th Iberian Conference on Information Systems and Technologies (CISTI)*, June, 16–19, 2010, Santiago de Compostela, Spain.

[16] S.G. Antunes, J.S. Silva and J.B. Santos, *A Level Set Segmentation Method of the Four Heart Cavities in Pediatric Ultrasound Images*, in *LNCS Imag. Anal. Rec.* **6112** (2010) 99.

[17] J. Santos, D. Celorico, J. Varandas and J. Dias, *Medical Interface for Echographic Free-hand Images*, *Int. J. Comput. Vision Biomech.* **3** (2008) 33.

[18] A. Ferreira, A.M. Morgado and J.S. Silva, *Automatic Corneal Nerves Recognition for Earlier Diagnosis and Follow-Up of Diabetic Neuropathy*, in *LNCS Imag. Anal. Rec.* **6112** (2010) 60.

[19] V. Vasconcelos, J.S. Silva, L. Marques and J. Barroso, *Statistical textural features for classification of lung emphysema in CT images: A comparative study*, in proceedings of *5th Iberian Conference on Information Systems and Technologies (CISTI)*, June, 16–19, 2010, Santiago de Compostela, Spain.

[20] C. Ferreira, B.S. Santos, J.S. Silva and A. Silva, *Comparison of a segmentation algorithm to six expert imagiologists in detecting pulmonary contours on x-ray CT images*, in *Med. Imag.* **5034** (2003) 347.

[21] R.C. Gonzalez and R.E. Woods, *Digital Image Processing*, 3rd Ed., Pearson Education, Inc. (2008).

[22] H. S.-C. Huang, *Anatomy of SUV*, *Nucl. Med. Bio.* **27** (2000) 643.

[23] B.S. Santos, C. Ferreira, J.S. Silva, A. Silva and L. Teixeira, *Quantitative evaluation of a pulmonary contour segmentation algorithm in x-ray computed tomography images*, *Acad. Radiol.* **11** (2004) 868.

[24] P. Annangi, S. Thiruvenkadam, A. Raja, H. Xu, X. Sun and L. Mao, *A region based active contour method for x-ray lung segmentation using prior shape and low level features*, in proceedings of *7th IEEE International Symposium on Biomedical Imaging (ISBI)*, April, 14–17, 2010, Rotterdam, Netherlands.

2013 JINST 8 C03018